Journal of Power Sources 188 (2009) 132–140

Contents lists available at ScienceDirect

Journal of Power Sources

journal homepage: www.elsevier.com/locate/jpowsour

Investigation of bio-inspired flow channel designs for bipolar plates in proton exchange membrane fuel cells

Jason P. Kloess[a], Xia Wang[b,*], Joan Liu[c], Zhongying Shi[b], Laila Guessous[b]

[a] Department of Mechanical Engineering, University of Michigan, Ann Arbor, MI, United States
[b] Department of Mechanical Engineering, Oakland University, Rochester, MI 48309, United States
[c] Department of Mechanical Engineering, Olin College of Engineering, MA, United States

ARTICLE INFO

Article history:
Received 6 October 2008
Received in revised form
24 November 2008
Accepted 25 November 2008
Available online 6 December 2008

Keywords:
PEM fuel cells
Bipolar plates
Flow channel design

ABSTRACT

Proton exchange membrane (PEM) fuel cell performance is directly related to the flow channel design on bipolar plates. Power gains can be found by varying the type, size, or arrangement of channels. The objective of this paper is to present two new flow channel patterns: a leaf design and a lung design. These bio-inspired designs combine the advantages of the existing serpentine and interdigitated patterns with inspiration from patterns found in nature. Both numerical simulation and experimental testing have been conducted to investigate the effects of two new flow channel patterns on fuel cell performance. From the numerical simulation, it was found that there is a lower pressure drop from the inlet to outlet in the leaf or lung design than the existing serpentine or interdigitated flow patterns. The flow diffusion to the gas diffusion layer was found be to more uniform for the new flow channel patterns. A 25 cm^2 fuel cell was assembled and tested for four different flow channels: leaf, lung, serpentine and interdigitated. The polarization curve has been obtained under different operating conditions. It was found that the fuel cell with either leaf or lung design performs better than the convectional flow channel design under the same operating conditions. Both the leaf and lung design show improvements over previous designs by up to 30% in peak power density.

1. Introduction

Polymer electrolyte membrane (PEM) fuel cells use pure hydrogen as a fuel and either pure oxygen or air as an oxidant to convert chemical energy of fuel directly into electrical energy through an electrochemical reaction. PEM fuel cells are the popular option for alternative power supply to the transportation system owing to their high power density, low operating temperature, low emission and compact design.

The average electric power from a single PEM fuel cell is limited to around 0.5 W cm^{-2} [1]. Hence several single PEM fuel cells must be stacked to make a fuel cell stack in order to create the desired power for various applications. To make a fuel cell stack, the components called bipolar plates are used to electrically, thermally, and physically connect the fuel cells and increase the power output. Another important feature of bipolar plates is that bipolar plates contain flow channels that distribute the fuel or oxidant evenly over the membrane electrode assembly (MEA). Meanwhile, the liquid water produced during the electrochemical reaction will be removed from the cell through the flow channels on the bipolar plate [2]. Therefore, the flow channel pattern on the bipolar plate plays a very important role in maintaining good performance of fuel cells.

Several existing flow pattern designs include the straight or parallel, single serpentine, triple serpentine, and interdigitated designs [3]. Each design has its own advantages and disadvantages that affect the fuel cell's performance differently. Much research work has been conducted to investigate the effects of various flow field designs on the performance of fuel cells [3–29]. The design of the flow channel on bipolar plates mainly focuses on three aspects: the flow channel distribution pattern [6–13], the cross-section shape [14–17] and the land and channel dimensions [15–22]. The gas is easily distributed in the straight or parallel fields. However, if a blockage should occur in one of the channels, the gas has alternate flow paths and therefore will not build up the pressure needed to force out the blockage [3,8]. The reactant distribution inside the cell is therefore not uniform either, which will result in a non-uniform local current density distribution. To solve this blockage problem, a single serpentine field is suggested. As the name implies, there is only one channel for the gas to flow, therefore forcing out water droplets and impurities. The entire channel length, however, is long compared to its cross-sectional area, thus creating a large pressure loss across the field. This leads to uneven diffusion into the gas diffusion layer (GDL) and can affect the long term performance of

* Corresponding author. Tel.: +1 248 370 2224; fax: +1 248 370 4416.
E-mail address: wang@oakland.edu (X. Wang).

0378-7753/$ – see front matter © 2008 Elsevier B.V. All rights reserved.
doi:10.1016/j.jpowsour.2008.11.123

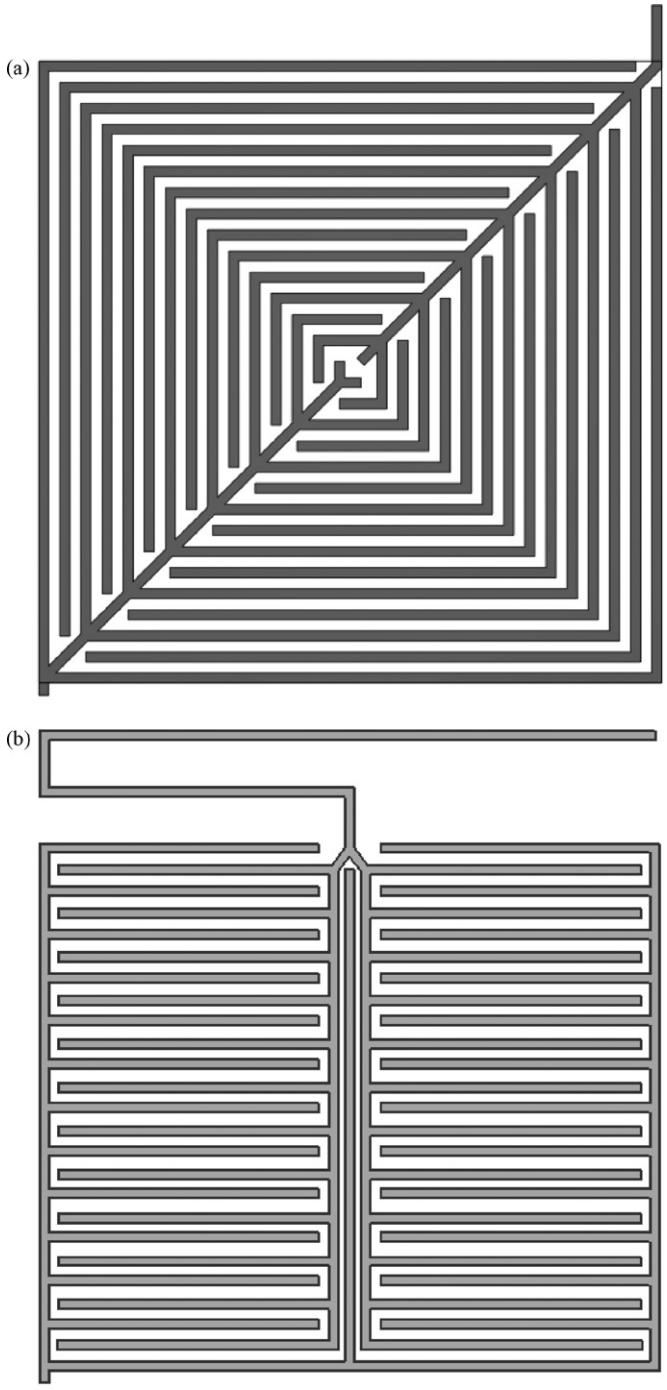

Fig. 1. (a) New bio-inspired leaf flow pattern. (b) New bio-inspired lung flow pattern.

the cell. On the other hand, the pressure difference between the adjacent channels causes the flow crossover from one channel to another channel which thus increases the convection of reactant in the GDL [23–27]. To improve the overall pressure loss in a single serpentine channel, a triple serpentine can be used [11]. In this design, three serpentine paths are connected at the inlet and outlet. However with the three channels, the pressure needed to remove water droplets or impurity blockages may not build up.

Another popular flow channel is the interdigitated pattern which uses a non-continuous set of inlet and outlet channels to force the gas through the GDL [9,28–29]. In interdigitated designs, the flow into the GDL is forced convection rather than diffusion. This helps avoid water build up and increases the limiting current density and maximum power by overcoming the limitations of diffusive mass transfer. The disadvantages, however, is that higher inlet pressures are required for operation, which leads to a high parasitic power loss for the fuel cell system to operate. Different from the aforementioned conventional designs, Morgan Fuel Cell also developed biomimetic plates, which show improvements in peak power by up to 16% using their biomimetic plates [3].

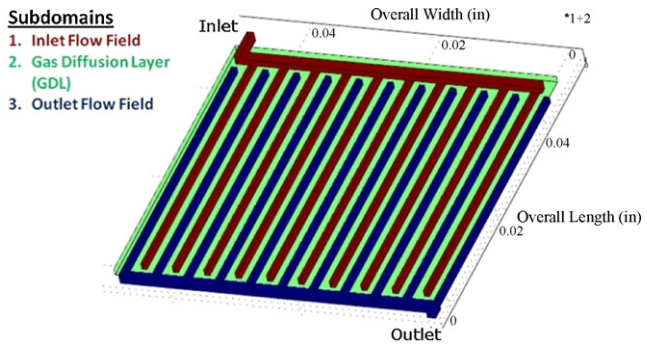

Fig. 2. Subdomains for interdigitated flow field used in simulation.

Much research is being done on flow fields and there are still opportunities to advance knowledge from its current state. The goal of this research is to develop new designs that combine the advantages of the existing patterns with inspiration from natural flow fields. In this investigation the natural flow fields chosen for two new designs were a lung layout and a leaf layout: a combination of the serpentine and interdigitated pattern geometries shown in Fig. 1a and b.

The objective of this paper is to evaluate the performance of two new bio-inspired flow pattern designs for bipolar plates in PEM fuel cells. A computational fluid dynamics (CFD) analysis was used to model the flow through the newly designed channels and diffusion into the GDL. The resulting pressure distribution and pressure loss is shown visually on the exchange boundary between the flow channel and GDL. Experimentally, the performance of the two existing designs and the new lung and leaf patterns were determined using a Fuel Cell Technologies test station. These bio-inspired plates demonstrate flow improvements as well as improved cell performance. The new designs show improved pressure distributions, decreased pressure loss, and increased cell performance in current density and peak power density compared to the single serpentine and interdigitated designs.

2. Computational model

2.1. Model assumptions and governing equations

Each design to be studied, including the single serpentine, interdigitated, lung, and leaf flow patterns, was physically modeled in Unigraphics NX4 and then imported as a parasolid to COMSOL Multiphysics 3.4. The flow is assumed to be steady, laminar, and incompressible in both flow channels and the gas diffusion layer. The fuel cell is assumed to operate isothermally. The momentum transport in a flow channel is governed by Navier–Stokes Eq. (1), and the momentum transport in the porous gas diffusion layer is governed by Brinkman's Eq. (2). The mass transport in both regions is governed by the continuity Eq. (3).

$$\rho\vec{u} \times \nabla\vec{u} = \nabla[-P\mathrm{I} + \mu(\nabla\vec{u} + \nabla\vec{u}^{\mathrm{T}})] \tag{1}$$

$$(\nu/\kappa)\vec{u} = \nabla\left[-P\mathrm{I} + \left(\frac{1}{\varepsilon}\right)\upsilon(\nabla\vec{u} + \nabla\vec{u}^{\mathrm{T}})\right] \tag{2}$$

$$\nabla \times \vec{u} = 0 \tag{3}$$

where ρ is the fluid density, kg m^{-3}, u is the velocity, m s^{-1}, P is pressure, Pa, μ is the fluid kinematic viscosity, m s^{-2}, κ is the permeability of gas diffusion layer, m^2, and ε is the porosity of the gas diffusion layer.

2.2. Model geometry and boundaries

In both the flow field and GDL subdomains, air is used as the working fluid. A constant temperature of 75 °C and the calculated pressure were used to establish the density and dynamic viscosity of the fluid. The GDL subdomain was connected to the flow field through a continuity boundary on the exchange surface between the GDL and flow field. For Brinkman's Eq. (2), a porosity of 0.78 and permeability of 1E−8 m^2 were used. Barbir has reported a permeability of 5–10 × 10^{-12} m^2 for carbon paper GDLs used in other simulations [30], however, the permeability in this model was increased to enhance the flow visualization though the GDL exchange surface. A GDL thickness of 1.016 mm was also used to enhance the flow visualization through the GDL exchange surface. The three subdomains (inlet flow field, outlet flow field, and GDL) are shown in Fig. 2 color coded by the legend for an interdigitated pattern design. A similar arrangement was used for the single serpentine, leaf, and lung designs.

Table 1
Input variables for computational model.

Variable name	Value	Description
T (°C)	75	Temperature
P_0 (Pa)	0	Initial pressure
E	0.78	Porosity of GDL
κ (m^2)	1E−8	Permeability of GDL
t_{gdl} (mm)	1.016	Thickness of GDL
v_i (m s^{-1})	20.75	Inlet velocity
P_o (Pa)	0	Outlet pressure (gage pressure)
w_c (mm)	0.7874	Flow field channel width
d_c (mm)	1.016	Flow field channel depth
w_r (mm)	0.8	Rib width

Four main boundary conditions were created for each flow pattern: inlet, outlet, walls, and GDL exchange. In the inlet boundary, the fluid velocity was given. In the outlet boundary, the outlet pressure was set to atmospheric pressure. A 'no-slip' condition was used for all of the wall boundaries. Finally, the Navier–Stokes Eq. (1) for the flow in the channel and Brinkman's Eq. (2) for the flow in porous

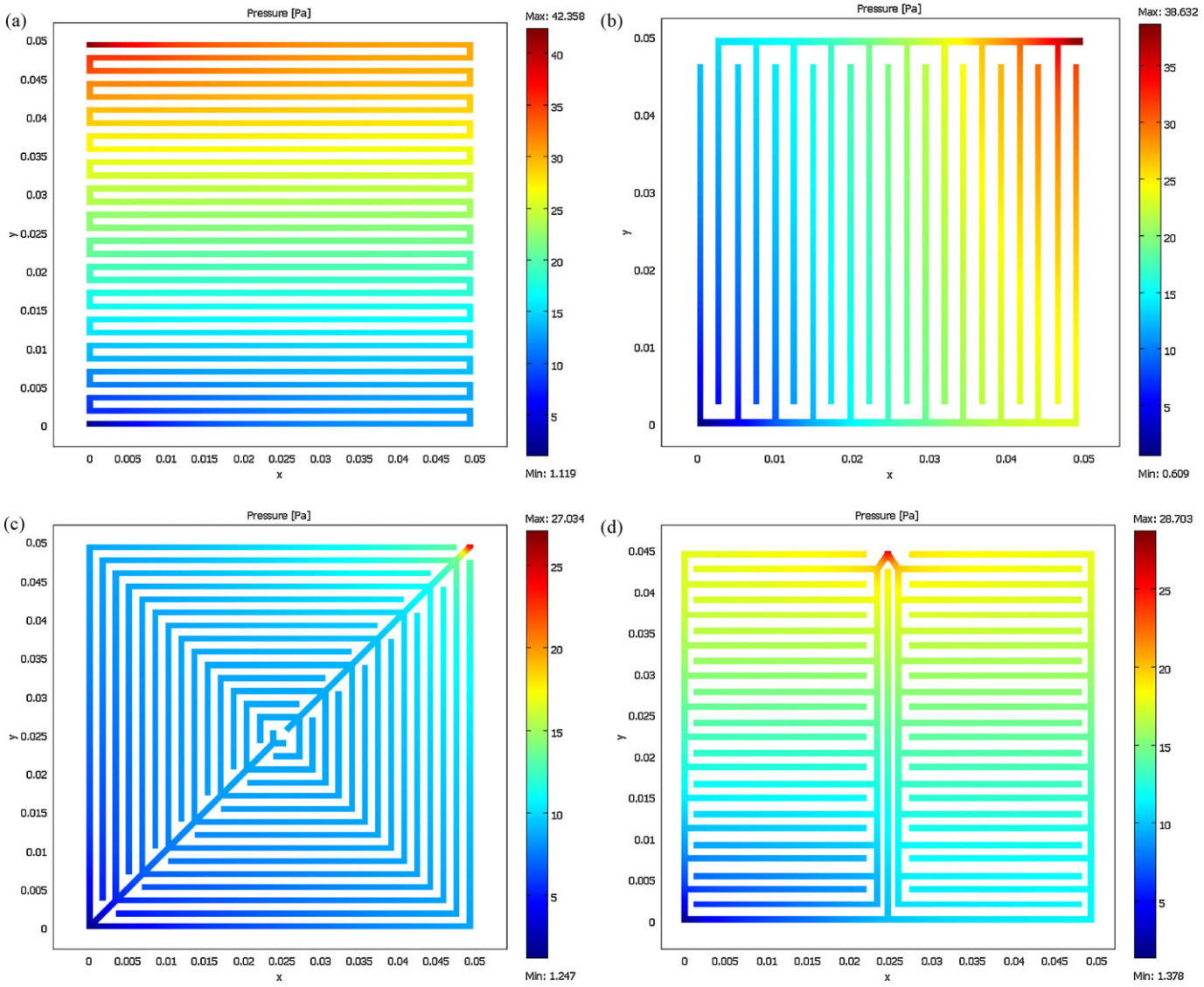

Fig. 3. (a) Pressure distribution in a single serpentine pattern. (b) Pressure distribution in an interdigitated flow pattern. (c) Pressure distribution in a leaf flow pattern. (d) Pressure distribution in a lung flow pattern.

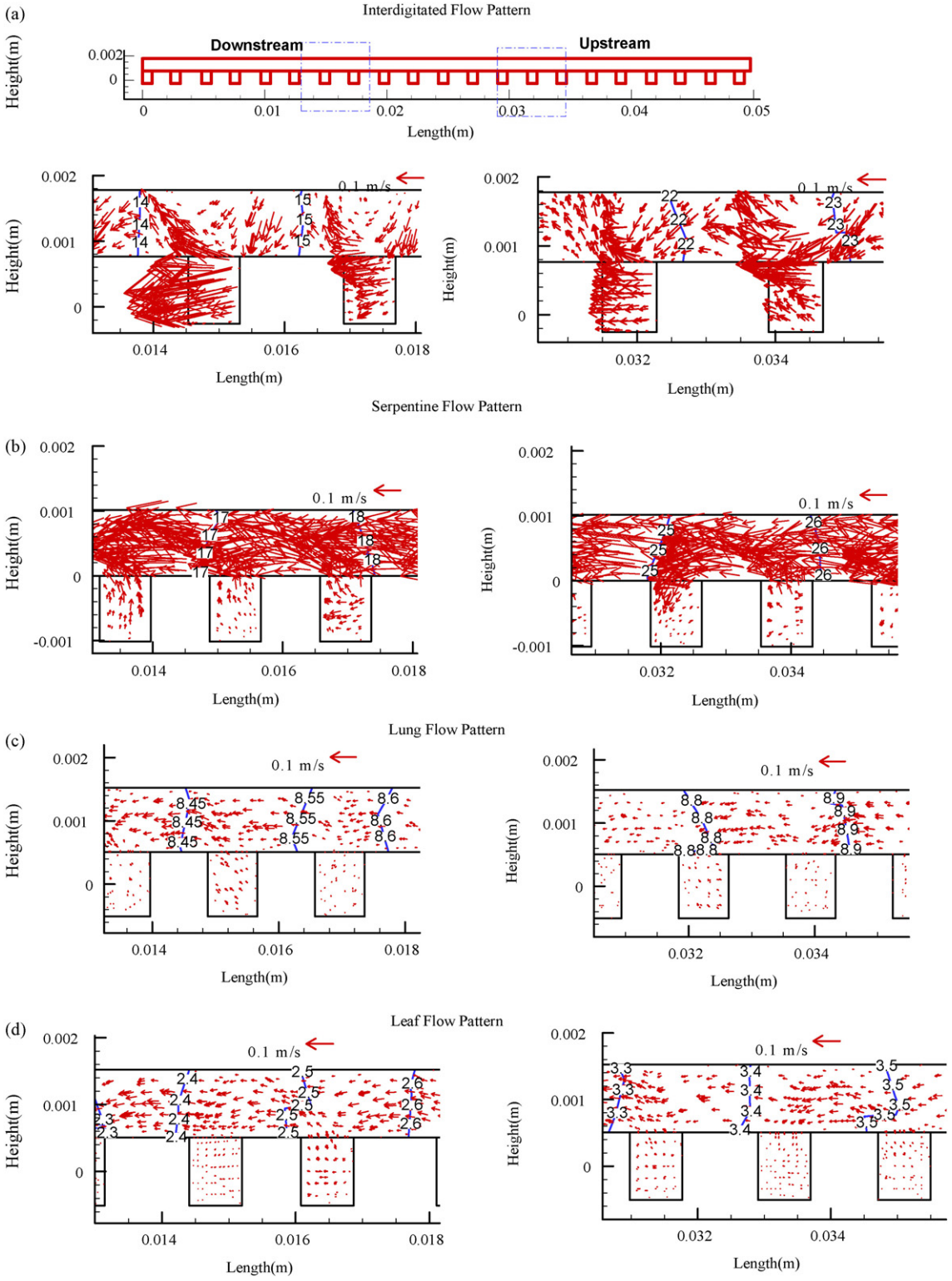

Fig. 4. Pressure distribution and velocity profile: the cut view in the middle of each design pattern.

gas diffusion layer are coupled along the interface between the GDL and channel through a 'continuity boundary' condition given as bellows:

$$\vec{u}_{NS} = \vec{u}_{Brinkman} \quad P_{NS} = P_{Brinkman} \tag{4}$$

Table 1 summarizes values and constants used in the computational model.

2.3. Simulation results and discussion

The SPOOLES solver (convergence tolerance = 1E−3 and maximum iterations = 100) in Comsol Multiphysics 3.4 was used to solve these equations for pressure and velocities in the three Cartesian axis directions. Pressure loss from the GDL input to output and the velocity normal to the GDL exchange surface were computed to assess the four designs.

Table 2
The computed pressure loss for various flow patterns.

Flow field	Pressure loss (Pa)
Single serpentine	41.23
Interdigitated	38.023
Leaf	25.794
Lung	27.325

The actual pressure drop the GDL input at the channel inlet to the output at the channel outlet is shown in Table 2. Fig. 3 shows the pressure distribution in different flow patterns. Both the leaf and lung patterns had an improved pressure loss over the single serpentine and interdigitated patterns. The values of the pressure drop for the single serpentine and interdigitated patterns are consistent with simulations performed by Karvonen et al. [31]. The pressure distributions along the GDL exchange were also more uniform in the new designs as illustrated in Fig. 3c and d. Both the leaf and lung designs result in less high pressure regions (shown in red) which help create a uniform diffusion into the GDL. The pressure distribution and the corresponding velocity profile were further examined by a cut view in the middle of each flow pattern design as shown in Fig. 4. A large magnitude of velocity is observed in both interdigitated and serpentine flow channels due to a large pressure drop. The velocity in both leaf and lung designs are relatively small but more uniform. Also, the pressure drop in both leaf and lung designs in the flow direction is much smaller than that in interdigitated and serpentine designs. The *Z* velocity contour profile in Fig. 5a–d, show that the diffusion through the GDL exchange surface is more uniform in the new leaf and lung designs and there are minimal spikes or dead zones that negatively affect the cell's performance. A high and uniform diffusion flow rate to the GDL will improve the fuel cell performance, which can be seen in next section.

3. Experimentation

In order to check the performance of new designs, four single PEM fuel cells are assembled with the serpentine flow pattern, interdigitated flow pattern, leaf flow pattern and lung flow pattern on the bipolar plates, respectively. The N112 membrane electrode assembly (MEA) from FuelCellStore.com was used for all the four designs with an anode and cathode loading of 0.5 mg Pt cm^{-2} each. This MEA performed well and produced consistent results over the extensive weeks of testing. In order to fabricate bipolar plate channels, a Computer-Controlled Bridgeport mill at Oakland University was used to cut the patterns on the high purity POCO© electrographite plates. In order to avoid any MEA damage or deformation, the bolt torques for each assembly were kept at a constant 120 in. lb

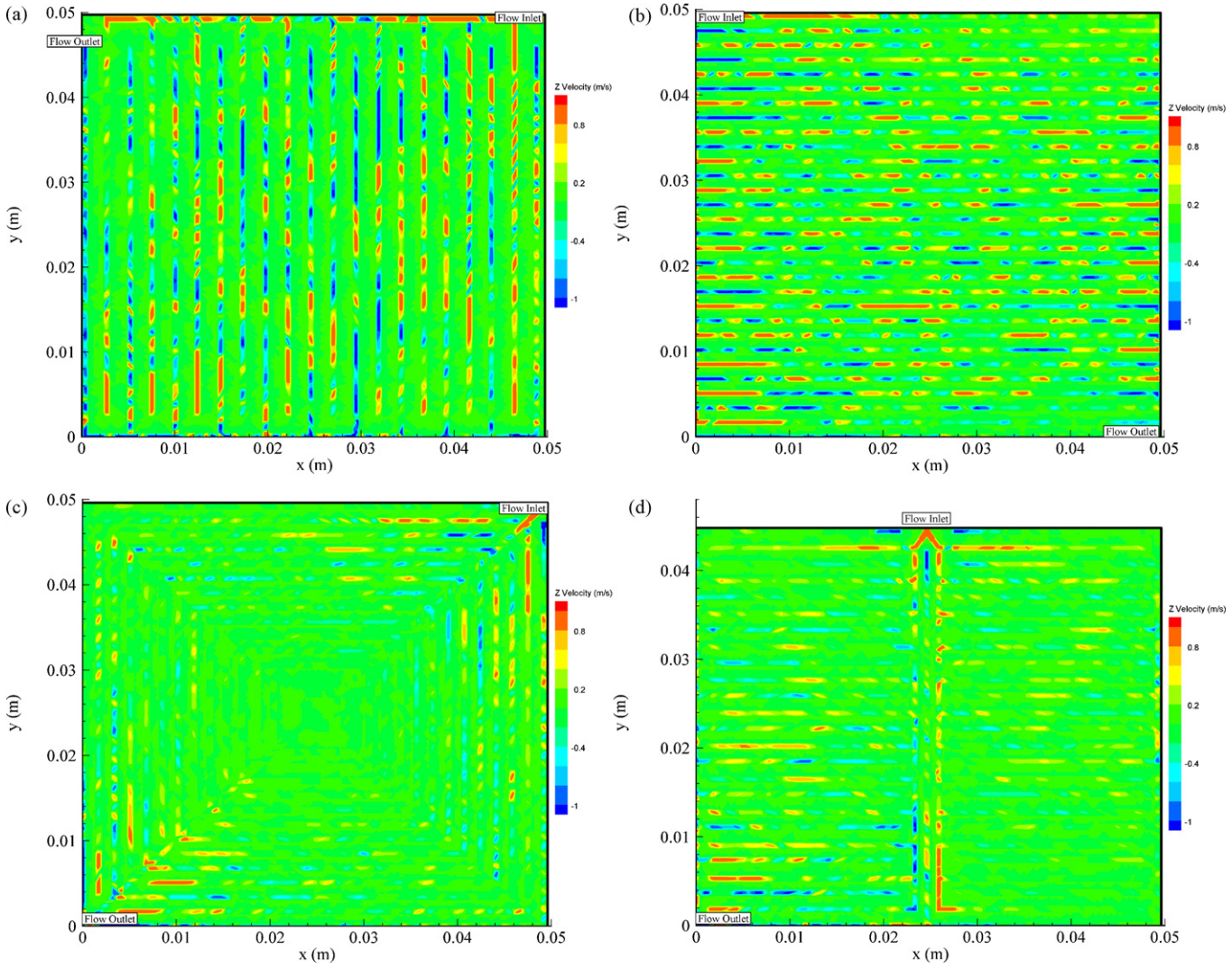

Fig. 5. (a) Contour profile of the *Z* velocity: interdigitated flow pattern. (b) Contour profile of the *Z* velocity: serpentine flow pattern. (c) Contour profile of the *Z* velocity: leaf flow pattern. (d) Contour profile of the *Z* velocity: lung flow pattern.

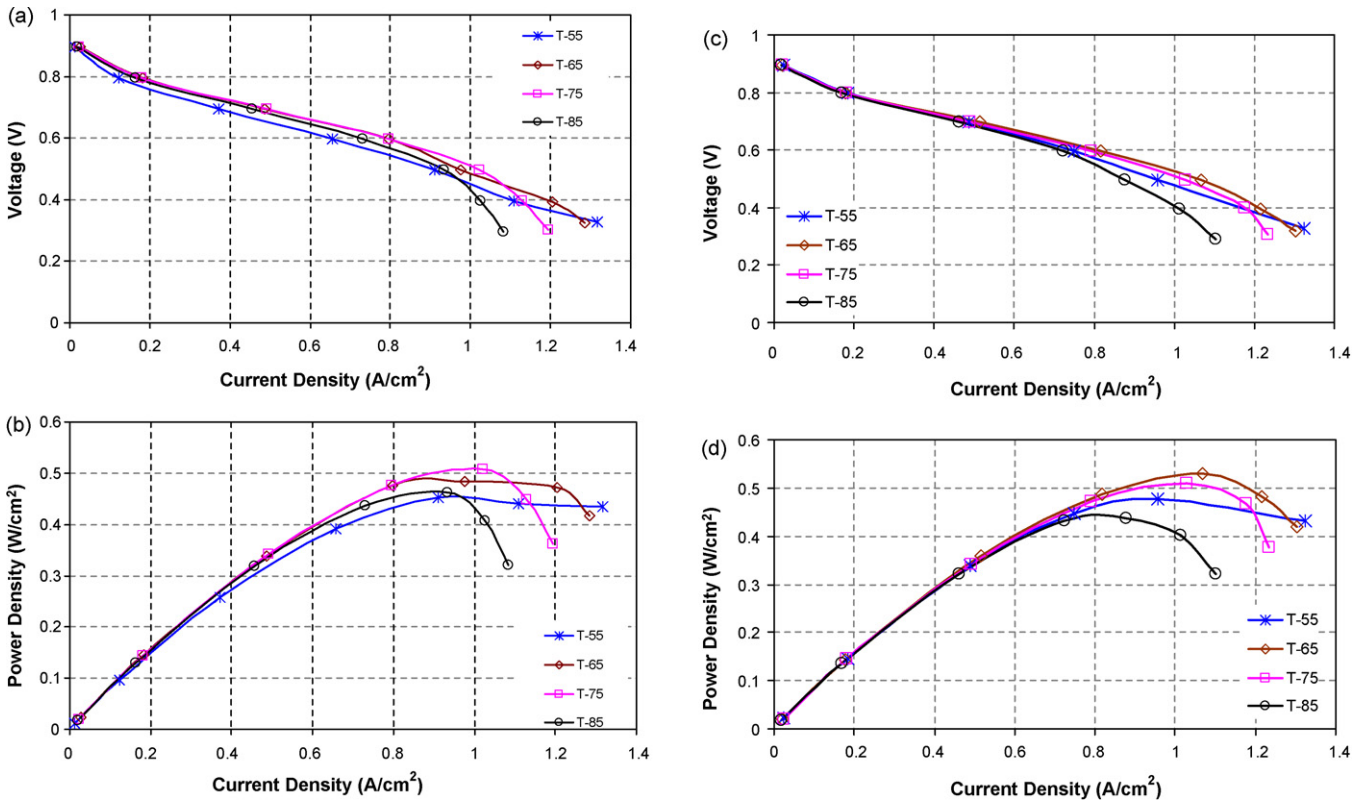

Fig. 6. (a) Leaf design: effects of operation temperature–polarization curve. (b) Leaf design: effects of operation temperature–power density. (c) Lung design: effects of operation temperature–polarization curve. (d) Lung design: effects of operating temperature–power density.

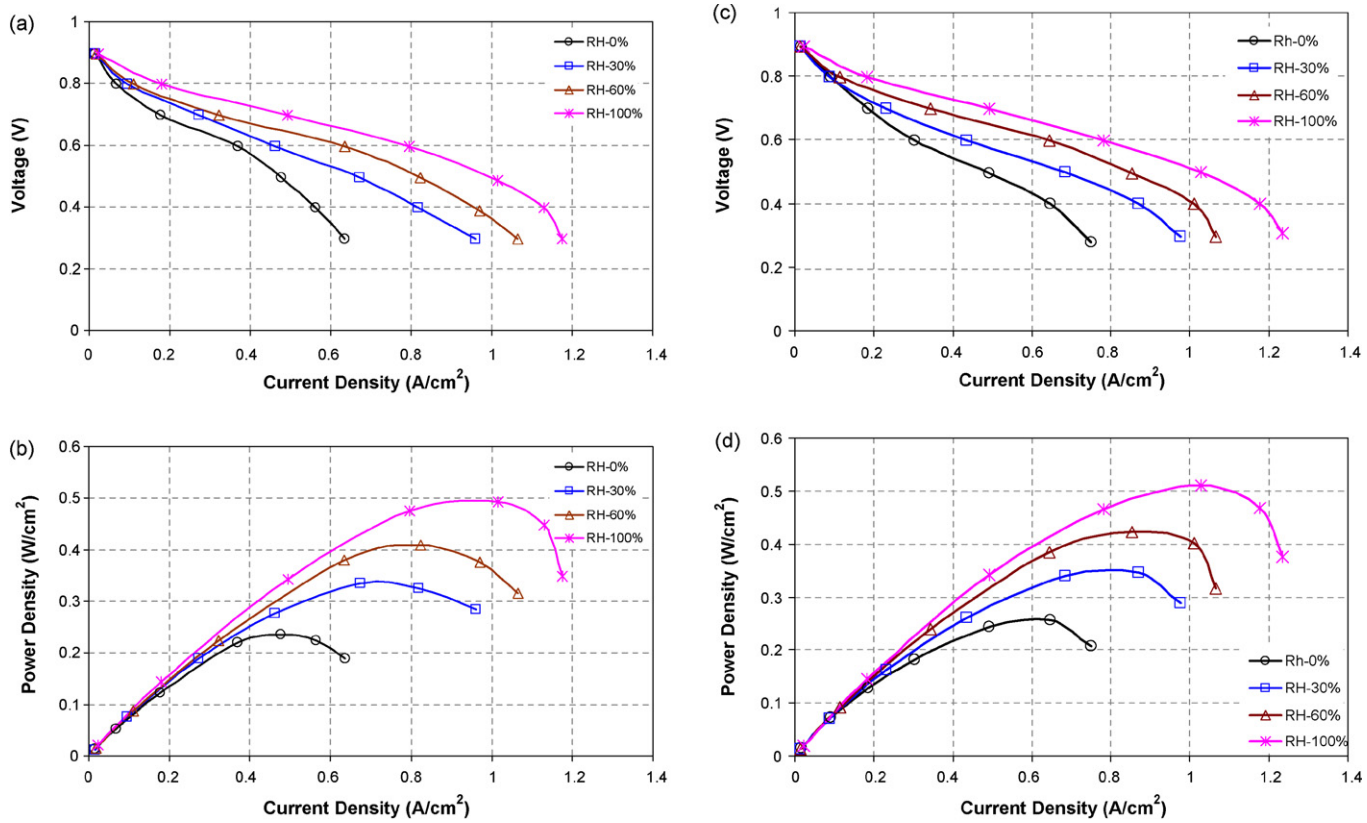

Fig. 7. (a) Leaf design: effects of relative humidity–polarization curve. (b) Leaf design: effects of relative humidity–power density. (c) Lung design: effects of relative humidity–polarization curve. (d) Lung design: effects of relative humidity–power density curve.

Table 3
Summary of testing conditions. For all test groups: anode: 99.9999% pure hydrogen; 300 sccm; cathode: compressed air: 1000 sccm.

	Temperatures (°C)	Back pressure (atm)	Relative humidity (anode:cathode)
Test Group 1: (temperature)	35	1	100%:100%
	55	1	100%:100%
	75	1	100%:100%
	85	1	100%:100%
Test Group 2: (pressure)	75	0	100%:100%
	75	1	100%:100%
	75	2	100%:100%
Test Group 3: (RH)	75	1	100%:0%
	75	1	100%:30%
	75	1	100%:60%
	75	1	100%:100%

using a beam deflection torque wrench. Previous tests [32] found this bolt torque value to be safe and high performing.

The University Model Test Station by the Fuel Cell Technologies Inc. was used to accurately measure the current density and voltage during testing. This test station maintains the inlet reactant temperature, cell temperatures, outlet backpressures, and inlet relative humidity. Except for the pressure regulators at the inlet, all of these conditions are altered and monitored using LabVIEW and recorded to a data sheet output.

Three test groups were performed to find optimum conditions for the new lung and leaf designs: cell temperature, relative humidity, and backpressures. In all of the groups, the anode and cathode pre-heaters were set to 5 °C higher than the anode and cathode humidifier temperatures to avoid condensation before the gas enters the fuel cell. During the backpressure tests, the tank regulators were increased from 30 psi to 60 psi in order to provide a sufficient pressure difference between the inlet and outlet. The test groups were also run in successive order with a cell purge between each test. For example during the temperature tests, the first test was at the lowest temperature while the final test was at the highest temperature. A similar progression was used for the relative humidity (0–100%) and backpressure (0–2 atm) experiments. The operating conditions summarized in Table 3, were repeated for each flow field design. The constant flow rates of 300 sccm ultra pure hydrogen and 1000 sccm compressed air are supplied to the anode and cathode electrode, respectively. A polarization plot of voltage (V) vs. current density ($A\,cm^{-2}$) and a power density ($W\,cm^{-2}$) vs. current density ($A\,cm^{-2}$) plot for all four patterns were used to show which design achieves the best performance and peak power density.

4. Experimentation results

4.1. Temperature effects

Fig. 6 shows the effects of operation temperature on the fuel cell with the new leaf and lung pattern design. The new leaf and lung designs show improvements in performance as temperature increases. This performance improvement peaks at 65–75 °C and then declines during the 85 °C test. One explanation for this is that at temperatures greater than 75 °C, the incoming water vapor does not hydrate the MEA well, but rather dries it out which decreases the performance. The reason is that the thermal couple in our test rig was located in the cathode end plate. Therefore, the real temperature in the membrane of the fuel cell should be a few degrees higher than the actual reading from the thermal couple due to heat loss from the metal end plates. During experimentation, it was also noticed that the gas at the exit was mostly water vapor at higher temperatures and more visible water droplets at lower temperatures. Since less water remains in the GDL at higher temperatures, the MEA can become dehydrated which thus decreases the performance of cell.

4.2. Relative humidity effects

Fig. 7 shows the effects of relative humidity at the inlet of the fuel cell on the cathode side. The new lung and leaf pattern designs

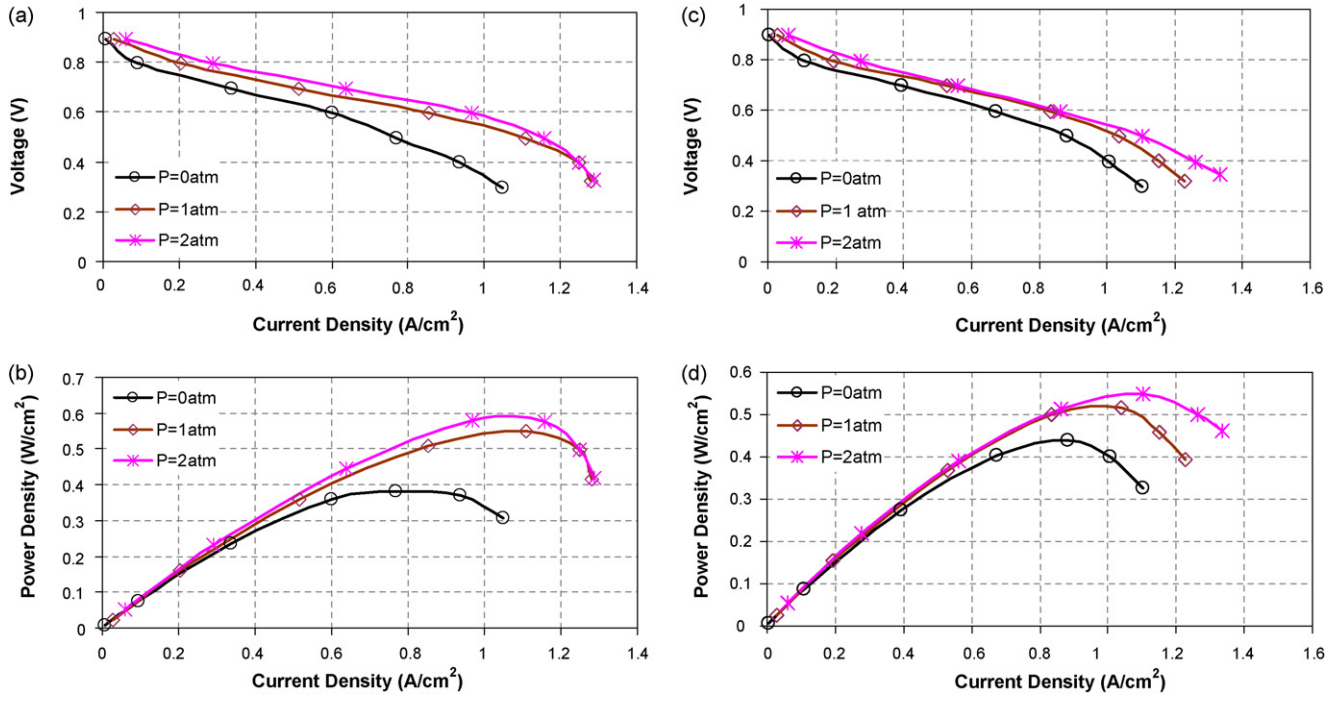

Fig. 8. (a) Leaf design: effects of operating pressure–polarization curve. (b) Leaf design: effects of operating pressure–power density. (c) Lung design: effects of operating pressure–polarization curve. (d) Lung design: effects of operating pressure–power density.

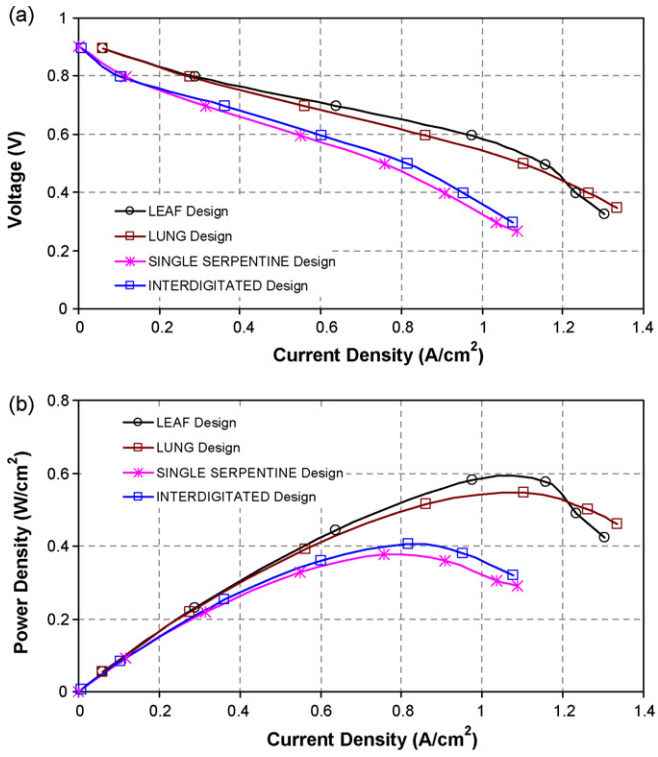

Fig. 9. (a) Polarization curve comparison for various flow pattern designs: $P = 2$ atm, $T = 75\,^{\circ}C$, RH = 100%. (b) Power density comparison for various flow pattern designs: $P = 2$ atm, $T = 75\,^{\circ}C$, RH = 100%.

follow a similar trend with an increase in cathode relative humidity. With a higher humidified oxidant, the membrane stays well hydrated, which facilitates the movement of electron from anode to cathode electrode. As a result, there is a low ohmic loss in the membrane as the humidity increases. A high current density is also achieved as the humidity increases. However, this trend also has a saturation point in the regions where water is readily produced from the high current demand. Water build up can occur; however, because it reaches the highest peak power density during the 100% humidity condition, this remains the optimum condition. This trend can be observed in Fig. 7a and b for the Leaf and Lung designs. The lung design shows a better performance than the leaf design under the same relative humidity. The maximum current density reached by the lung design a little higher. The lung design removes water more easily than the leaf design considering its symmetrical parallel design feature.

4.3. Backpressure effects

Fig. 8 shows the effects of backpressure at the outlet of the fuel cell. During the test, the backpressure was maintained to be the same on both anode and cathode sides. As pressure increases, the fuel cell performs better with either a leaf or lung design. This increase in performance is very obvious when the backpressure increases from 0 atm to 1 atm, and it is not so obvious when the backpressure increases from 1 atm to 2 atm. This is consistent with the founding for the fuel cell with an interdigitated channel design [28]. The reaction rate is increased because that more oxidant is available at higher pressures and forced into the GDL more readily. However, one drawback with increasing the backpressure is that water can build up due to a lower pressure differential between the inlet and outlet, which causes unsteady test results. An optimum backpressure of 2 atm is shown in Fig. 8a and b for the leaf and lung designs; however, frequent purges were needed to remove water for the higher reaction rate.

4.4. Performance comparison between the serpentine, interdigitated, leaf and lung designs

Serpentine, interdigitated, leaf, and lung designs are compared at the same operating conditions: backpressure of 2 atm, temperature of 75 °C, and a relative humidity of 100%. As shown in Fig. 9, the new leaf and lung designs show improvement in overall performance and peak power density by up to 30% compared to either the serpentine or interdigitated design. The leaf design has the best performance followed by the lung, interdigitated and single serpentine design.

5. Conclusions

In PEM fuel cells, bipolar plates are major components that physically, electrically, and thermally connect the cell together to produce electrical power. Flow patterns on these bipolar plates significantly affect the immediate and long term performance of the fuel cell. This research shows promising results for bio-inspired flow patterns with noticeable improvements in pressure loss, overall performance, and peak power density. The optimum operating conditions of 65–75 °C cell temperature, 2 atm backpressure, and 100% relative humidity are found for the new leaf and lung designs. Under these operating conditions, the leaf design has the best performance of the two. Both the leaf and lung design show improvements over previous designs by up to 30% in peak power density.

To achieve further improvements, the following should be investigated: tapered ends, rounded corners, and surface treatment of the plates. Tapered ends may further improve the pressure loss on each channel as shown in previous research. Although milling may be difficult, rounded corners may help create more uniform flow through the channels and thus more consistent diffusion into the GDL. Heat surface treatment of the plates will create a more uniform surface and possibly lower the contact resistance between the MEA and bipolar plate. Future work with these PEM fuel cells includes a transparent endplate fuel cell in order to visualize the water build up inside the cell. This transparent fuel cell will clearly show any areas of water or impurity build up and suggest possible improvements to the designs tested.

Acknowledgements

Support for this research came from the 2008 Automotive Research and Industrial Mentorship (ARIM) Research Experience for Undergraduates Program at Oakland University, Rochester, Michigan. The program is supported by National Science Foundation (Grant Number: 0552737). Special thanks are extended to Lab Manager Len Brown, Project Engineer Pete Taylor, and Graduate Student Assistant Elaine Petrach for their help with machining and testing.

References

[1] H.J. Hograth Warren, J.B. Benziger, J. Power Sources 159 (2006) 969–978.
[2] A. Turhan, K. Heller, J.S. Brenizer, M.M. Mench, J. Power Sources 180 (2) (2008) 773–783.
[3] X. Li, I. Sabir, Int. J. Hydrogen Energy 30 (2005) 361–370.
[4] F. Barreras, A. Lozano, L. Valiño, C. Marín, A. Pascau, J. Power Sources 144 (2005) 54–66.
[5] F. Chen, Y.Z. Wen, H.S. Chu, W.M. Yan, C.Y. Soong, J. Power Sources 128 (2004) 125–134.
[6] W.M. Yan, H.C. Liu, C.Y. Soong, F. Chen, J. Power Sources 161 (2006) 907–919.
[7] C. Xu, T.S. Zhao, Electrochem. Commun. 9 (2007) 497–503.
[8] A. Su, Y.C. Chiu, F.B. Weng, Int. J. Energy Res. 29 (2005) 409–425.
[9] D.L. Wood, J.S. Yi, T.V. Nguyen, Electrochim. Acta 43 (1998) 3795–3809.
[10] E. Birgersson, M. Vynnycky, J. Power Sources 153 (2006) 76–88.

[11] S. Kim, S. Shimpalee, J.W. Van Zee, J. Electrochem. Soc. 152 (6) (2005) A1265–A1271.
[12] S. Perng, H. Wu, J. Power Sources 175 (2008) 806–816.
[13] S. Shimpalee, S. Greenway, J.W. Van Zee, J. Power Sources 160 (2006) 398–406.
[14] A. Kumar, R.G. Reddy, J. Power Sources 113 (2003) 11–18.
[15] H.C. Liu, W.M. Yan, C.Y. Soong, F. Chen, H.S. Chu, J. Power Sources 158 (2006) 78–87.
[16] L. Sun, P.H. Oosthuizen, K.B. McAuley, Int. J. Therm. Sci. 45 (2006) 1021–1026.
[17] W. Sun, B.A. Peppley, K. Karan, J. Power Sources 144 (2005) 42–53.
[18] X. Wang, Y. Duan, W. Yan, X. Peng, Electrochim. Acta 53 (2008) 5334–5343.
[19] X. Wang, Y. Duan, W. Yan, X. Peng, J. Power Sources 175 (2008) 397–407.
[20] S.Y. Hwang, H. Joh, M. Aulice Scibioh, S. Lee, S. Kim, T.G. Lee, H.Y. Ha, J. Power Sources 183 (2008) 226–231.
[21] W. Yan, H. Li, P. Chiu, X. Wang, J. Power Sources 178 (2008) 174–180.
[22] W.M. Yan, C.Y. Soong, F. Chen, H.S. Chu, J. Power Sources 125 (2004) 27–29.
[23] J.P. Feser, A.K. Prasad, S.G. Advani, J. Power Sources 161 (2006) 404–412.
[24] J. Park, X. Li, J. Power Sources 163 (2007) 853–863.
[25] P.H. Oosthuizen, L. Sun, K.B. McAuley, Appl. Therm. Eng. 25 (2005) 1083–1096.
[26] M.V. Williams, H.R. Kunz, J.M. Fenton, J. Electrochem. Soc. 151 (2004) A1617–A1627.
[27] Z. Shi, X. Wang, J. Power Sources 185 (2) (2008) 985–992.
[28] L. Wang, H. Liu, J. Power Sources 134 (2004) 185–196.
[29] S. Yi, T.V. Nguyen, J. Electrochem. Soc. 146 (1999) 38–45.
[30] F. Barbir, PEM Fuel Cells: Theory and Practice, Academic Press, New York, 2005.
[31] S. Karvonen, T. Hottinen, J. Sarrinen, O. Himanen, J. Power Sources 161 (2006) 876–884.
[32] W. Lee, C.H. Ho, J.W. Van Zee, M. Murthy, J. Power Sources 84 (1999) 48–50.